JOURNAL OF GEOPHYSICAL RESEARCH, VOL. 113, C10014, doi:10.1029/2008JC004750, 2008

A coastal current in winter: 2. Wind forcing and cooling of a coastal current east of Cape Cod

Andrey Y. Shcherbina[1,2] and Glen G. Gawarkiewicz[1]

Received 28 January 2008; revised 26 May 2008; accepted 21 July 2008; published 18 October 2008.

[1] The combined effect of cooling and wind-driven buoyancy flux (WDBF) on a buoyant coastal current east of Cape Cod is investigated using observations and process-oriented numerical modeling. Theoretical considerations show that with the moderately strong surface density gradients observed in the Outer Cape Cod Coastal Current, WDBF can substantially exceed the buoyancy loss due to cooling, especially during intense winter storms. Evidence of deep convection associated with strong negative WDBF during downwelling-favorable winds is clearly seen in the moored observations. A simplified two-dimensional numerical model is used to illustrate the evolution of wind- and buoyancy-driven cross-shelf overturning circulation in response to surface cooling and episodic storm events. The simulation confirms that WDBF plays an important role in driving subduction of cold surface water at the offshore surface outcrop of the coastal current font. The presence of the coastal current is also shown to block onshore Ekman transport. As a result, the downwelling circulation in a cross-shore plane is predicted to have a complex multicell structure, in which exchange between the inner shelf and midshelf is restricted. The downwelling circulation has a major impact on the cross-shelf origin of cold, dense shelf waters contributing to intermediate layers of the Wilkinson Basin of the Gulf of Maine.

Citation: Shcherbina, A. Y., and G. G. Gawarkiewicz (2008), A coastal current in winter: 2. Wind forcing and cooling of a coastal current east of Cape Cod, *J. Geophys. Res.*, *113*, C10014, doi:10.1029/2008JC004750.

1. Introduction

[2] Buoyant coastal currents are a common feature in the coastal ocean [*Hill*, 1998]. River and estuarine outflows typically act as sources of buoyancy that drive these currents. Cross-shelf widths and velocity scales of coastal currents vary depending on the strength of the outflows and alongshore distance [*Garvine*, 1996]. Recent theoretical work has established the effects of a sloping bottom on the structure and advective scale of the flow [*Lentz and Helfrich*, 2002].

[3] Wind forcing of buoyant plumes has been a subject of much recent interest. *Fong and Geyer* [2001] have shown how the surface Ekman layer interacts with the plume and affects mixing. *Lentz* [2004] has extended these results to include continuity effects from the entire plume, and *Lentz and Largier* [2006] have examined the impact of wind forcing on the Chesapeake Bay plume. Enhancement of turbulent mixing by wind-driven shear has been addressed in a number of studies [*Fong and Geyer*, 2001; *Hetland*, 2005; *Whitney and Garvine*, 2005]. *Houghton et al.* [2004] have also used dye releases to study mixing within wind-forced plumes. Most of these studies have focused on the periods of peak freshwater input, typically late spring or summer, when heat fluxes are either positive or negligible and vertical stratification is relatively strong.

[4] The plume dynamics become more complicated in winter, when the strong negative buoyancy forcing is combined with wind-driven effects. The Outer Cape Cod Coastal Current (OCCC) is an example of a system where the joint effects of buoyancy input due to river runoff, buoyancy loss due to atmospheric cooling, and wind forcing may become important. OCCC is a continuation of the western Maine coastal current (WMCC) [*Fong et al.*, 1997; *Franks and Anderson*, 1992; *Geyer et al.*, 2004]. In a previous study [*Shcherbina and Gawarkiewicz*, 2008], OCCC was found to persist through the winter on the shallow shelf east of Cape Cod, an area affected by substantial cooling and periodic northeasterly winter storms.

[5] In this study we examine the response of the Outer Cape Cod Coastal Current to the seasonal cooling and downwelling-favorable wind forcing. Field observations used in this study are briefly presented in section 2. In section 3 recent theories for wind-driven buoyancy effects for the deep ocean are reviewed and applied to the case of a coastal current. Observations supporting theoretical considerations are also presented, and a quantitative comparison is made between the wind-driven buoyancy flux and the air-sea heat flux. A process-oriented numerical model is used to examine the secondary circulation near the coastal current and the interaction of the wind-driven surface mixed layer

[1] Woods Hole Oceanographic Institution, Woods Hole, Massachusetts, USA.
[2] Now at Applied Physics Laboratory, University of Washington, Seattle, Washington, USA.

0148-0227/08/2008JC004750$09.00

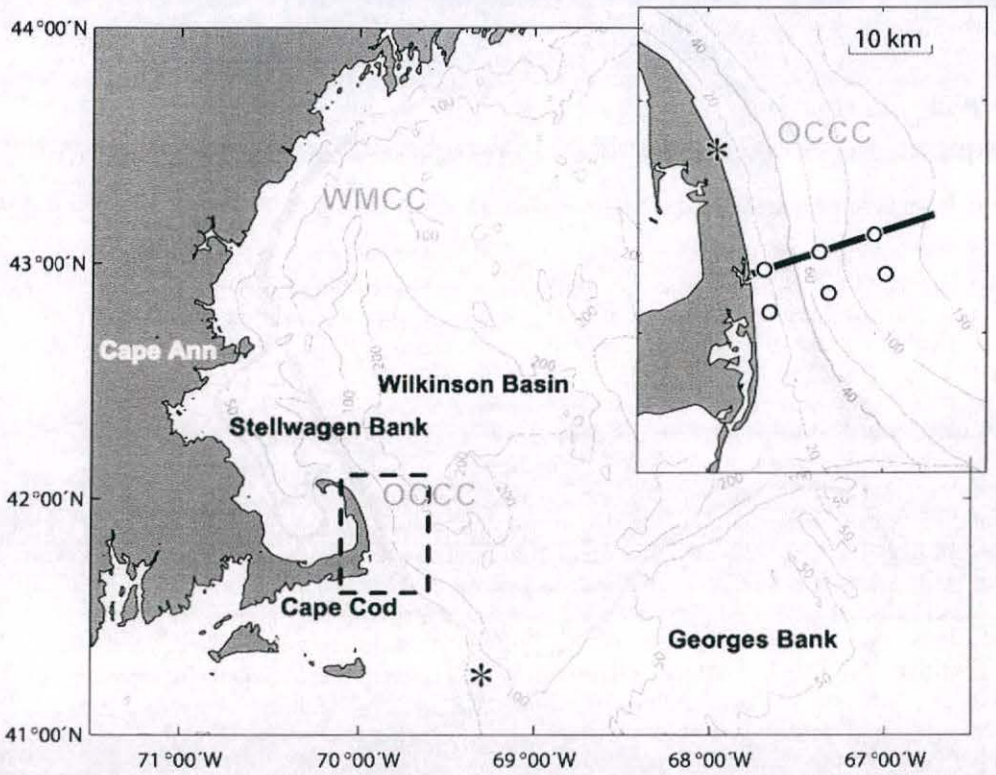

Figure 1. Map of the southwestern Gulf of Maine. The dashed box marks the Outer Cape Cod region, also shown on the inset. The inset shows the location of the mooring array (circles). The cross-shore hydrographic section is shown by black line. Asterisks mark the locations of meteorological observations. Gray arrows show the schematics of the coastal current system, including the Western Maine Coastal Current (WMCC) and Outer Cape Coastal Current (OCCC).

with the coastal current circulation in section 4. The discussion in section 5 focuses on the implications of the cooling and cross-shelf circulation on the formation of cold water masses that contribute to lateral advective cooling of the intermediate layers of the Gulf of Maine. Finally, a brief summary is given in section 6.

2. Outer Cape Cod Coastal Current Experiment

[6] The present study focuses on the shelf east of Cape Cod, Massachusetts (Figure 1). The experimental domain extended approximately 15 km offshore and spanned the depth range of 10–120 m.

[7] Wintertime processes on the Outer Cape Cod shelf were studied during 2005–2007, combining moored, shipboard and autonomous underwater vehicle hydrographic observations. A well-developed Outer Cape Cod Coastal Current (OCCC), an extension of the Western Maine Coastal Current, persisted in the area throughout the observation period. A detailed account of the coastal current structure and its evolution during the winter based on autonomous underwater vehicle (AUV) observations is given in the preceding paper [*Shcherbina and Gawarkiewicz*, 2008]. Here we give a brief overview of hydrographic structure of the plume and ambient shelf waters during the winter.

[8] The cross-shelf thermohaline structure observed on the Outer Cape Cod shelf in winter was dominated by a wedge of relatively fresh OCCC water near the coast (Figure 2). Density stratification was almost entirely determined by salinity; temperature increased with increasing depth. The offshore extent of OCCC water was marked by a relatively weak thermohaline front, which typically intersected the bottom between the 40- and 60-m isobaths and outcropped at the surface near the 100 m isobath. The slope of the front varied greatly over the winter in response to changing wind forcing and salinity within the plume.

[9] The present study focuses on moored, shipboard, and meteorological observations made in the OCCC area, described in the following sections.

2.1. Moorings

[10] The mooring array consisted of 6 moorings, placed at the 17-, 60-, and 120-m isobaths, approximately 7 km apart (Figure 1, Table 1). A pair of moorings was deployed at each of these three isobaths, forming two parallel cross-shelf lines, offset by 5 km. The moorings were deployed on 19 December 2005 with R/V *Tioga* and recovered on 21 March 2006. Light-duty mooring hardware was used, consisting of 60–130 kg pyramid anchors, 1-m diameter Polyform A floats, and a combination of 14 mm synthetic Amsteel rope and 17 mm chain.

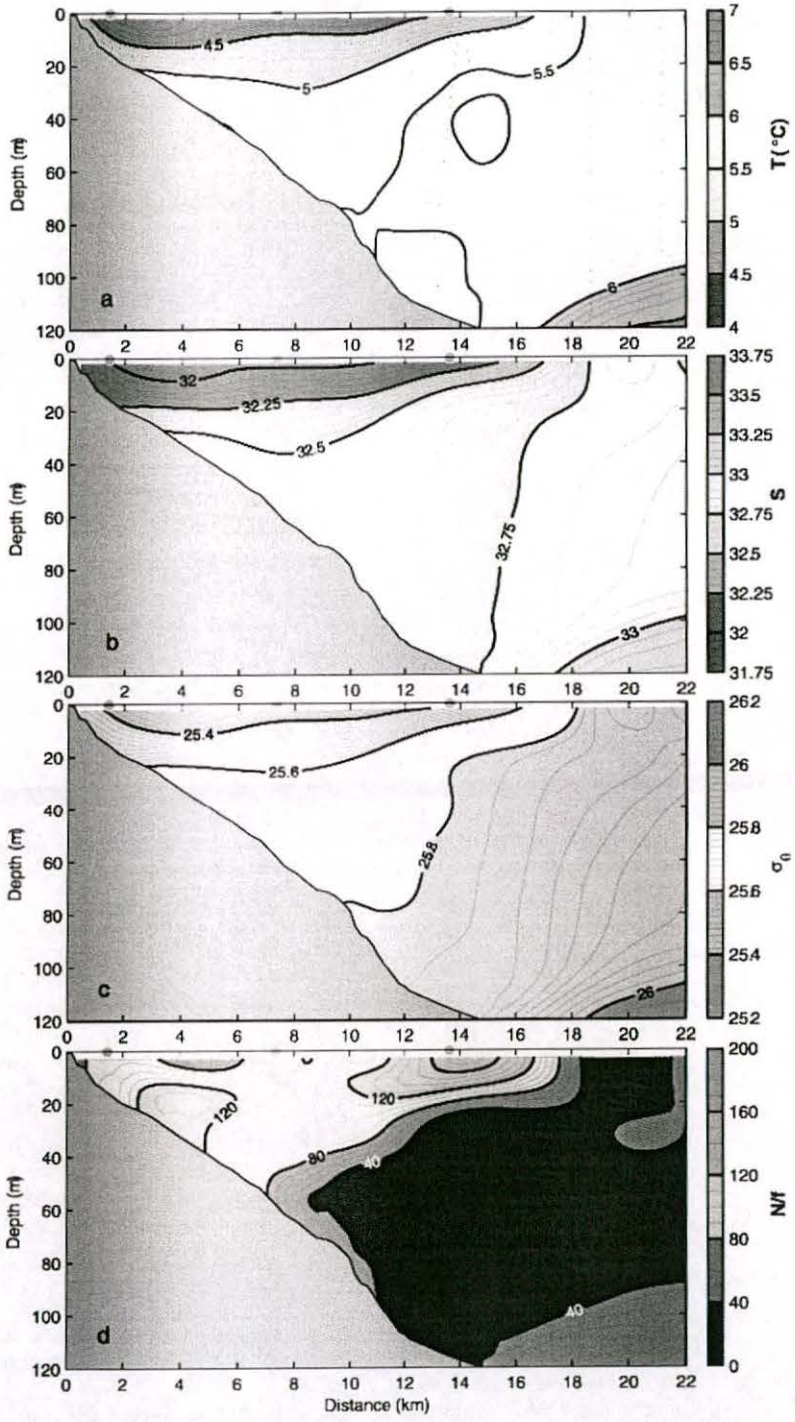

Figure 2. Distribution of (a) temperature, (b) salinity, (c) potential density, and (d) buoyancy frequency (normalized by the Coriolis parameter f) on a cross-shelf section occupied on 15 February 2006 with an autonomous underwater vehicle (AUV) and shipboard conductivity-temperature-depth (CTD) casts. The AUV trajectory and locations of CTD casts are shown by dotted lines in Figure 2a. Red circles mark the location of temperature moorings.

Table 1. Summary of the 2006 Mooring Deployment[a]

Mooring	Location	Depth (m)	Offshore distance (km)	Equipment
1 M17	41°49.171′N, 69°55.291′W	17.7	1.4	WTP (3)
2 M60	41°50.131′N, 69°51.218′W	60.6	7.4	WTP (7)
3 M120	41°51.262′N, 69°46.941′W	120	13.6	WTP (13)
4	41°46.441′N, 69°54.593′W	17.0	1.9	WTP (1), Tidbit(2)
5	41°47.218′N, 69°51.153′W	60.2	6.8	WTP (1), Tidbit(6)
6	41°48.539′N, 69°46.202′W	120	14.1	WTP (7), Tidbit (6)

[a]WTP, Water Temp Pro.

[11] Each mooring was equipped with temperature recorders fixed to the line at a 10-m vertical interval (total of 46 recorders). Two types of recorders were used: StowAway Tidbit, and HOBO Water Temp Pro (WTP) manufactured by Onset Computer Corporation. Both units have the same nominal accuracy (0.2°C), but the newer WTP provides better resolution (0.02°C versus 0.16°C for Tidbit). All instruments were set up to sample synchronously at 5-min time intervals.

[12] Special care was taken to ensure maximum consistency of the temperature measured by the inexpensive temperature probes. All units were equilibrated simultaneously in an ice bath prior to the deployment. In the absence of an independent temperature standard, the actual bath temperature was approximated by the mean of the sensor readings $t_0 = -0.036$°C. Temperature corrections relative to t_0 were established for each sensor and used during the processing of the field data. All the corrections were well within the specified accuracy of the instruments: the mean absolute correction was 0.03°C for WTPs and 0.1°C for Tidbits. The accuracy of temperature records, calibrated against their own mean in this fashion, likely exceeded that of the individual measurements (assuming some degree of randomness of the instrument errors). It was also likely to be more accurate than a calibration based on assuming the bath to be at the freezing point of fresh water ($t_0 = 0$°C), since the latter depends on ice and water purity. However, no claims of quantitative accuracy improvement could be made. Nominal instrument drift for the duration of the experiment was expected to be negligible (0.03°C).

[13] Results obtained on the northern and southern mooring lines were qualitatively similar, indicating that the alongshore decorrelation scale of the temperature field was substantially longer than the 5-km separation between the lines. Consequently, only the northern moorings, instrumented predominantly with WTPs, were used in the analysis, unless mentioned otherwise. The three moorings are referred to as "M17" (inshore, 17-m isobath), "M60" (middle, 60-m isobath), and "M120" (offshore, 120-m isobath).

2.2. Shipboard Observations

[14] Underway hydrographic observations accompanied every cruise of R/V *Tioga* which was used for deployment and recovery of both the AUV and the mooring array. Flow-through sampling of near-surface water was performed using the onboard SeaBird MicroTSG Thermosalinograph. Even though the MicroTSG employs highly accurate temperature and conductivity sensors, the accuracy of the system as a whole is compromised by the largely unknown effects of the ship's plumbing and lack of regular calibration data.

[15] For the present study, underway MicroTSG observations were cross-calibrated with the concurrent data obtained by the AUV, as well as the occasional conductivity-temperature-depth casts. As a result of such calibration, the linear regressions of the "true" temperature and salinity on the values reported by the thermosalinograph were established and used to correct the underway observations. Standard deviation of the regression residuals were 0.055°C and 0.025 for temperature and salinity, respectively.

2.3. Heat Flux Observations

[16] Heat flux on the Outer Cape Cod shelf is strongly seasonal and remains negative for 5.5 months out of the year. Climatological monthly mean heat loss derived from global objectively analyzed air-sea fluxes [*Yu et al.*, 2004] reach -185 W m^{-2} in December and -169 W m^{-2} in January (Figure 3).

[17] Characteristics of the air-sea heat exchange can vary considerably in the nearshore zone [*Smith and MacPherson*, 1987]. Consequently, both the coastal and offshore sources of meteorological data were considered for this study. The closest land-based meteorological station was located 17 km northwest of the middle of the mooring array in Wellfleet, MA. It is a commercial weather station operated by WeatherFlow, Inc. Simultaneous open ocean observations were available at the NOAA's National Data Buoy Center (NDBC) station #44018, located 80 km southeast of the experiment site.

[18] Wellfleet observations appear to have been heavily influenced by coastal effects. The wind speed observed at this station was typically less than half of that reported by the offshore buoy [*Shcherbina and Gawarkiewicz*, 2008]. On the other hand, temperature variability observed at the coast was stronger than at the offshore buoy by about 40%. Both data sets were used for estimation of heat fluxes, as the atmospheric forcing on the shelf is expected to vary between the two extremes. Heat fluxes were estimated using the Tropical Ocean-Global Atmosphere experiment / Coupled Ocean-Atmosphere Response Experiment (TOGA/COARE) bulk air-sea flux algorithm [*Fairall et al.*, 2003].

[19] Heat loss during the 2005–2006 winter, estimated using offshore data was similar to the climatological average (Figure 3). Maximum heat loss during the winter of 2005–2006 was 260 W m^{-2}, observed in December at the offshore weather buoy. Typical heat loss in January–February was 160 W m^{-2}, somewhat larger than the long-term mean. By the end of March the heat flux became positive. Heat loss based on coastal observations was typically 50–100 W m^{-2}

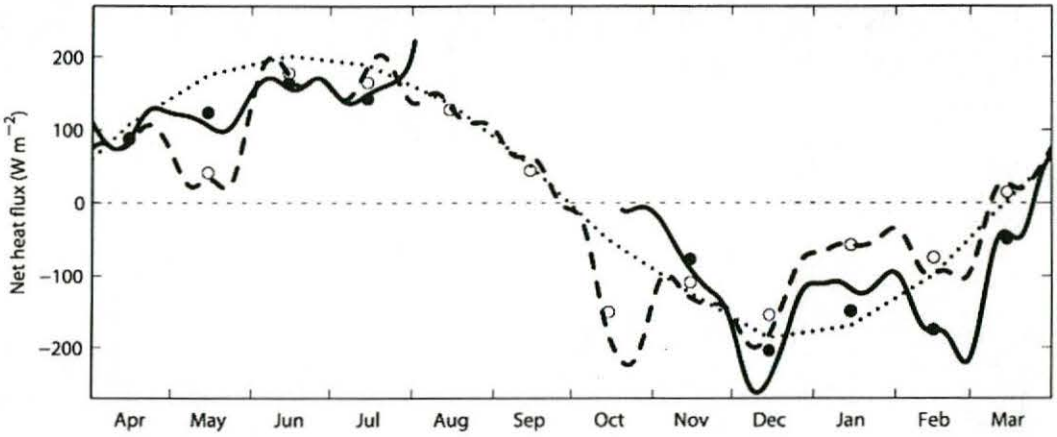

Figure 3. Net air-sea heat flux in April 2005 to March 2006. Heat flux was calculated using Tropical Ocean-Global Atmosphere / Coupled Ocean-Atmosphere Response Experiment (TOGA/COARE) bulk algorithm, with local meteorology (dashed line) and offshore buoy observations (solid line). Hourly observations were smoothed with a 15-day Blackman filter. Monthly means of local and offshore heat flux are shown by open and closed circles, respectively. The local climatological mean for 1984–2002 is shown by the dotted line. Gray shading represents the 2006 experiment duration.

smaller during December 2005 to March 2006. About half of the difference can be attributed to the water at the offshore buoy being 1–2°C warmer than near the coast.

3. Wind-Driven Convection

[20] Destabilizing effects of wind-driven advection of buoyancy have been previously studied in the context of open ocean fronts [*Straneo et al.*, 2002; *Thomas*, 2005]. In the following sections we will examine this effect in a coastal current setting, using the OCCC as an example.

3.1. Wind-Driven Buoyancy Flux

[21] We start with a brief recap of the theory, following [*Straneo et al.*, 2002] and [*Thomas*, 2005]. Consider the secondary circulation adjacent to the coast induced by an alongshore wind stress τ_y (Figure 4). We will be mostly interested in the near-surface flow, concentrated within the Ekman layer of thickness d. According to Ekman theory, the vertically integrated cross-wind volume transport within this layer is

$$U_E = \frac{\tau_y}{f\rho_0},$$

where f is the Coriolis parameter, and ρ_0 is the reference density. In the presence of a cross-shelf buoyancy gradient

$$\frac{\partial b}{\partial x} \equiv -\frac{g}{\rho_0}\frac{\partial \rho}{\partial x},$$

which is assumed vertically uniform within the Ekman layer, the volume transport leads to cross-shore divergence of buoyancy transport

$$B_E = -U_E\frac{\partial b}{\partial x} = \frac{gU_E}{\rho_0}\frac{\partial \rho}{\partial x}. \quad (1)$$

The divergence of buoyancy transport can be seen as a wind-driven buoyancy flux (WDBF) imposed at the surface and equal to B_E.

[22] In a typical coastal current associated with a buoyant plume density increases away from the coast heading offshore ($\partial\rho/\partial x > 0$). Downwelling-favorable wind ($U_E < 0$) then leads to onshore Ekman transport of denser water, corresponding to negative WDBF. During the winter, when vertical stratification is already weakened by cooling, such buoyancy loss would reduce water column stability and instigate vertical overturning.

3.2. Observations of Coastal Current Cooling Progression

[23] As evident from the moored observation, cooling of shelf waters off Outer Cape Cod was not uniform during the 2005–2006 winter (Figure 5). Most noticeable is the difference in the evolution of vertical temperature stratification. At M17, the inshore mooring, the water column was typically well-mixed (temperature differences on the order of the measurement accuracy) throughout the winter. In

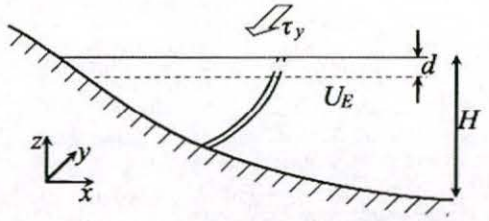

Figure 4. Schematic diagram of wind-driven buoyancy advection at the coastal current front (double line). The case of southward (downwelling favorable) wind stress τ_y is shown. The horizontal dashed line represents the extent of Ekman layer of thickness d. Ekman transport U_E is directed toward the shore (horizontal arrows). H is the total water depth.

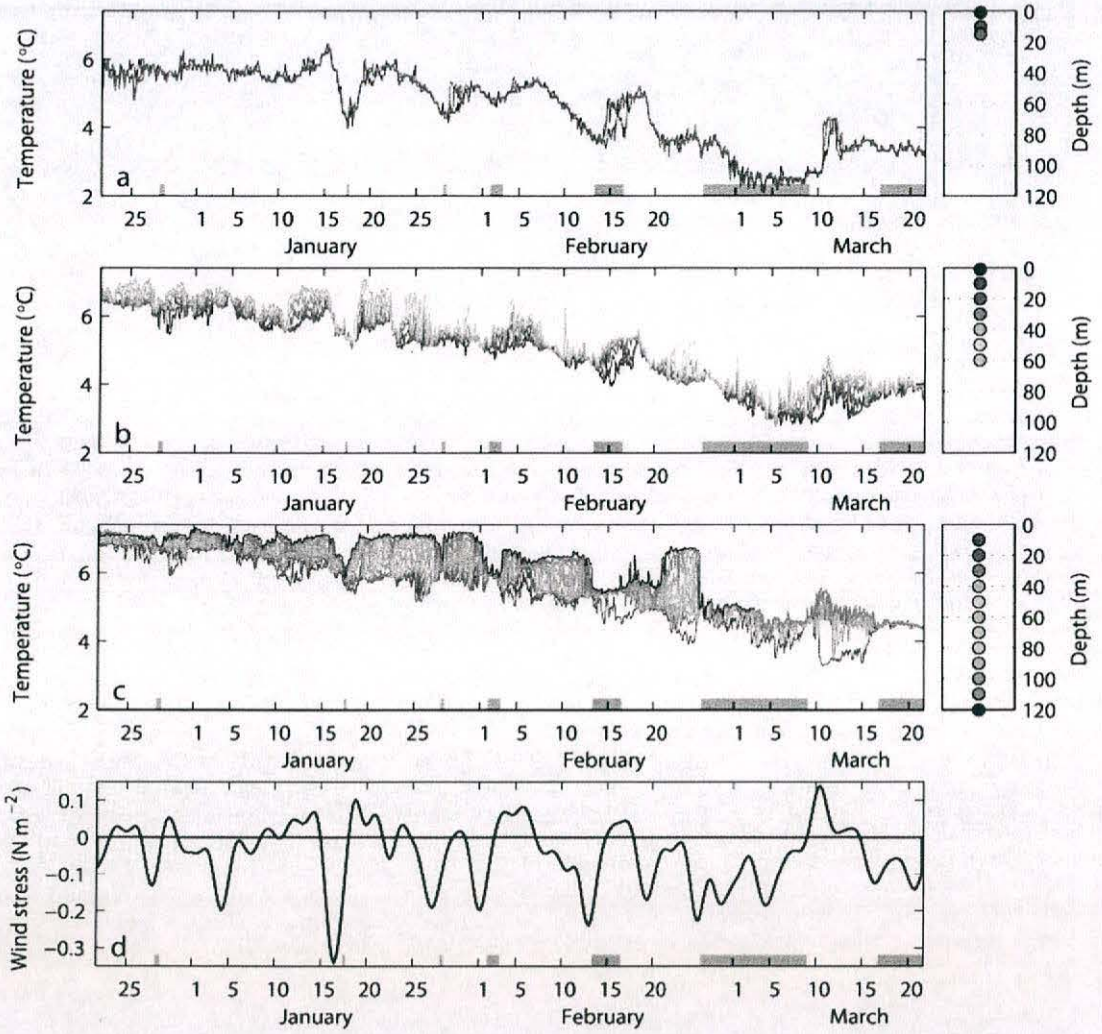

Figure 5. Temperature time series at moorings (a) M17, (b) M60, and (c) M120. Observations at 22 temperature sensors are shown, color-coded by nominal deployment depth of each. Vertical distribution and color-coding of sensor locations are also shown. (d) Low-passed alongshore wind stress. Positive values correspond to southerly (upwelling favorable) winds. Horizontal bars in Figures 5a, 5b, 5c, and 5d indicate periods of decreased stratification at M120 location.

contrast, the water remained predominantly stratified at the M60 and M120 sites, with the temperatures at the surface 1–3°C lower than at the bottom.

[24] During the February–March 2006, several periods of apparent deep convection were registered at the M120 mooring (Figure 5c): 2–3 February, 13–16 February, 25 February to 9 March, and 16–22 March. During these events, vertical temperature stratification between 40 and 120 m at this site was rapidly reduced. On 25 February 2006, the temperature difference between the 120- and 10-m horizons dropped from 2.7°C to less than 0.5°C over the period of 14 h. Earlier in the season (e.g., 4–5 January, 15–18 January), similar but shallower convection events were observed at the M60 mooring (Figure 5b). Most deep convection episodes were associated with the downwelling-favorable winds, prevalent in winter (Figure 5d), and were likely driven by a combination of WDBF and cooling. The relative importance of these two main destabilizing processes is examined in section 4. During the brief relaxation periods of neutral and upwelling-favorable winds, stratification was temporarily restored.

[25] Another noticeable feature of stratification dynamics was a periodic decrease in temperature registered at 10-m depth relative to the rest of the water column. This deviation was most pronounced at M120 mooring site (reaching −1.6°C on 10 March 2006), but was also synchronously present at the other two moorings (Figure 5). Because of the strong salinity influence, stratification likely remained stable despite negative vertical temperature gradients. Emergence of the cold surface layer typically coincided with upwelling-favorable or neutral winds. The behavior of this layer appeared to be decoupled from that of the deeper layers; it was found overlaying both stratified (e.g., 22–24 February) and well-mixed (e.g., 14–18 February,

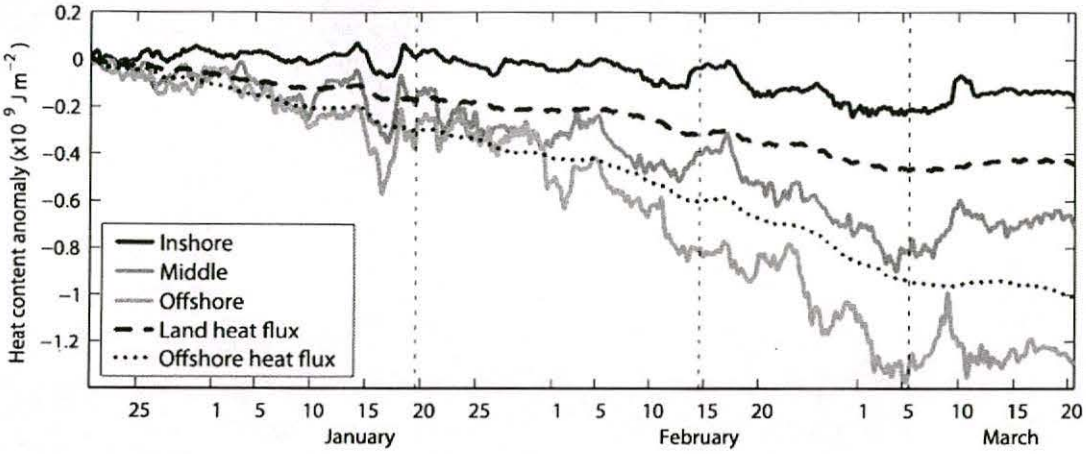

Figure 6. Heat content evolution at the inshore (blue), middle (green), and offshore (orange) moorings. Cumulative heat loss based on land (dashed) and offshore (dotted) observations are shown for comparison. Vertical dotted lines mark the time of the cross-shelf surveys shown in Figure 7.

10–15 March) waters. Strong contrast between the temperature at 10- and 40-m horizons and association with upwelling-favorable winds suggested Ekman advection of colder coastal water over the mooring site as a possible explanation of these observations. Note also that during these upwelling events the water column at the M17 (inshore) mooring became stratified, indicating the arrival of warmer water in the bottom layer (Figure 5a).

[26] It should be noted that the wind observations occasionally failed to predict the periods of upwelling and downwelling, evident in the mooring record. In particular, the downwelling and restratification cycle that took place on 13–25 February appears to be out of phase with the wind. The discrepancy can be attributed to the spatial separation between the site of the wind observations and the mooring location. The timing mismatch of individual weather events between the experiment site and the weather buoy 80 km southeast is not surprising. Overall stratification trends, however, agree reasonably well with the observed wind forcing.

[27] Analysis of the integral heat balance suggests an advective cross-shelf redistribution of heat. In the absence of advection, the surface heat loss balances the change in net water column heat content

$$\zeta = \int_{-H}^{0} \rho c_p T dz,$$

where H is the water depth, c_p is the specific heat capacity of seawater, and T is the temperature. The rates of heat content decrease observed at the three mooring sites were systematically different (Figure 6). The net heat loss was the weakest in shallow water, while increasing by a factor of 6 toward offshore. This increase was also about twice the difference between the coastal and offshore observations of heat fluxes (while occurring over much shorter spatial separation). Consequently, it could not be attributed to the spatial variation of heat loss and must indicate strong cross-shelf heat redistribution. The heat exchange was likely associated with wind-driven secondary circulation, rather than with baroclinic eddy activity, as no sign of the latter was observed. The structure of the wind-driven circulation in the cross-shelf plane and the ways it is affected by WDBF are further investigated in section 4.

3.3. Comparison of WDBF With Surface Buoyancy Loss

[28] Ekman-driven buoyancy transport in the surface mixed layer is difficult to observe directly, but an estimate based on (1) can be made. Between 21 December 2005 and 21 March 2006, 5 cross-shelf transects along the northern mooring line (Figure 1) were occupied with R/V *Tioga*. On the basis of underway TSG observations of surface temperature and salinity (section 2.2), cross-shelf density gradients were estimated (Figure 7). As expected, the strongest gradients were observed 6–10 km offshore, where the coastal current front intersected the surface. Negative density gradients near the shore were due to cooling in the shallowest waters but did not have a significant impact on the structure of the coastal current and will not be considered here.

[29] WDBF at the coastal current front was then estimated by applying (1) to the maximum near-surface buoyancy gradient observed during each survey. Alongshore wind stress observed during the transects was not representative of the typical wind forcing east of Cape Cod. Because of the harsh winter conditions, field operations were limited to the periods of fair weather, which were typically associated with southerly (upwelling favorable) winds. Through the winter, the predominant wind direction, however, was northerly (downwelling favorable) [*Shcherbina and Gawarkiewicz*, 2008]. To account for wind stress variability, 2-week averages of wind stress centered on the day of each transect were used to characterize typical cross-shore Ekman transport U_E, and, subsequently, B_E. Estimated negative WDBF increased from 1.2 and 0.5 $\times$ 10^{-7} m^2 s^{-3} in December and January to over 3 $\times$ 10^{-7} m^2 s^{-3} in March. This increase was brought about by both the sharpening of

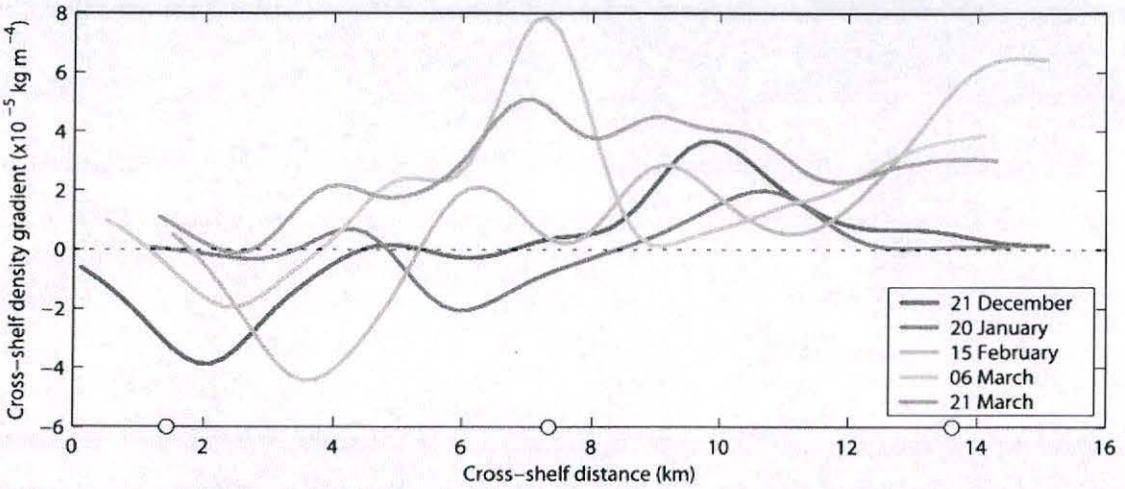

Figure 7. Low-passed cross-shelf density gradients, based on underway observations in December 2005 to March 2006. Circles mark the locations of the moorings.

the density gradient (Figure 7) and the intensification of downwelling wind forcing in late winter.

[30] The destabilizing effect of wind-driven advection of buoyancy can be compared with the direct surface cooling, which has been considered to be the only mechanism responsible for deep convection on an ice-free shelf. The surface buoyancy flux associated with the heat flux Q is

$$B_Q = \frac{g\alpha}{\rho_0 c_p} Q,$$

where α is the thermal expansion coefficient, and c_p is the specific heat capacity of seawater. East of Cape Cod, seasonal cooling produces only moderate buoyancy loss of 5×10^{-8} m^2 s^{-3}. Consequently, wind-driven buoyancy advection is expected to dominate the buoyancy budget at the CC front in February–March by a large margin (Figure 8).

[31] By increasing the density at the surface and destabilizing the water column, both the cooling-related and the wind-driven buoyancy fluxes act in a similar manner. Spatial and temporal characteristics of these effects, however, are very different. Surface heat loss typically varies on the scale of weather systems (tens to hundreds of kilometers), and only weakly depends on local variation of sea surface properties. On the other hand, the WDBF effect is highly localized to the regions of strong surface density gradients; it also depends on the appropriate alignment of these gradients with the Ekman transport. Even though the large-scale average contribution of WDBF is far weaker than that of surface heat loss, it can dominate locally under

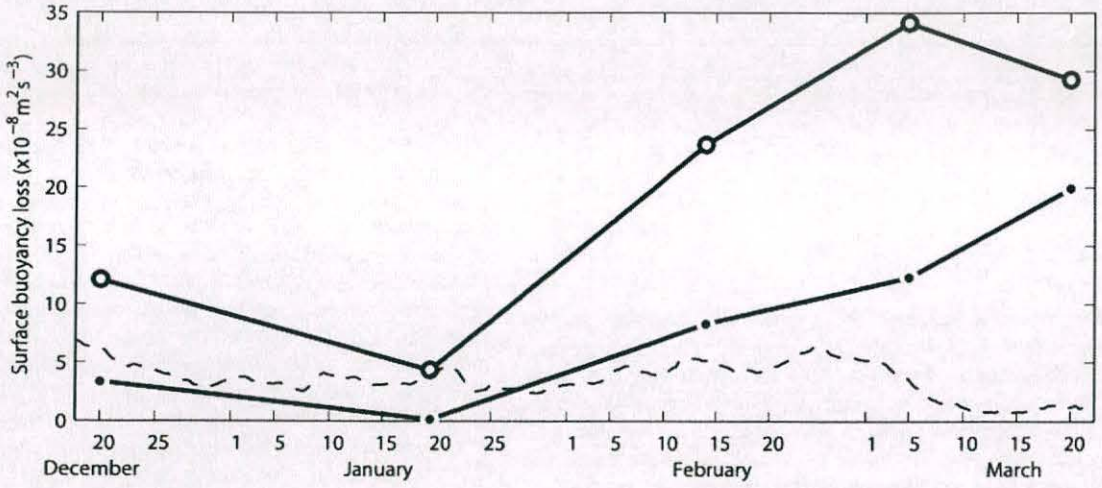

Figure 8. Negative wind-driven buoyancy flux in the coastal current, estimated using (1) with the observed maximum (open circles) and mean (solid circles) surface density gradients and 2-week wind stress averages. A dashed line shows the buoyancy loss due to direct cooling, estimated from the offshore buoy observations and smoothed with a 2-week running average filter.

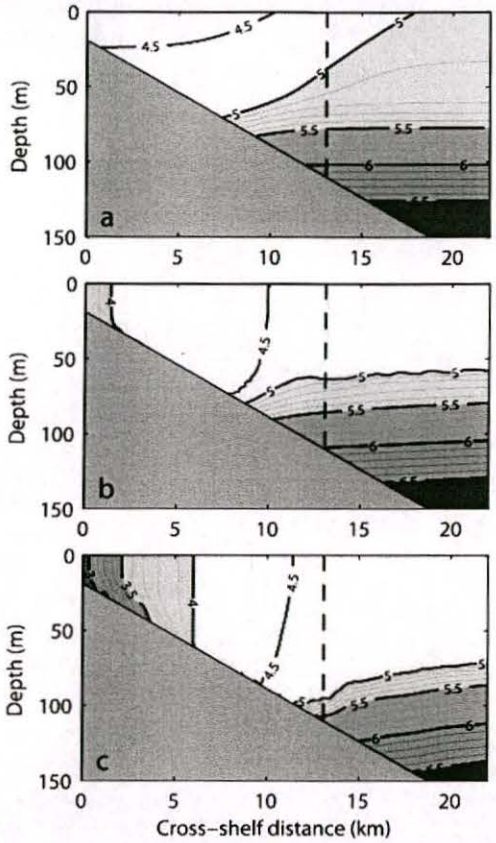

Figure 9. Evolution of cross-shelf temperature structure under the influence of constant cooling and periodic downwelling. (a) Initial temperature distribution (day 0) and snapshots at the peaks of two successive wind events (days (b) 5 and (c) 12) are shown. Details of temperature evolution at the virtual mooring site marked with a dashed line is shown in Figure 10.

favorable conditions (such as those observed at the Outer Cape Cod shelf in early spring). As shown in section 4 below, such localized influence can produce substantial changes in cross-shelf circulation patterns and water mass exchange. The relative proximity to the shore sets the midshelf coastal current WDBF apart from the similar effect at open ocean fronts discussed by *Straneo et al.* [2002] and *Thomas* [2005]. Horizontal density gradients observed at OCCC are considerably stronger than those found in open-ocean fronts. Our study showed a maximum density gradient of 8×10^{-5} kg m^{-4} (Figure 7). *Straneo et al.* [2002] report a maximum horizontal density gradient of 3.3×10^{-6} kg m^{-4} within the Labrador Current, with the mean mixed layer density gradient of 2.5×10^{-6} kg m^{-4}. At the same time, typical wintertime surface heat loss in the temperate latitudes of Cape Cod (100–200 W m^{-2}) is weaker than in the subarctic Labrador Current (400–600 W m^{-2}). Consequently, the destabilizing effect of WDBF can be expected to be considerably more pronounced on the shelf. On average, the ratio of wind-driven buoyancy flux across the OCCC front to the vertical buoyancy flux during December 2005 to March 2006 on the Cape Cod shelf (5:1) is about 1 order of magnitude greater than that estimated for the Labrador Current (0.32) [*Straneo et al.*, 2002].

[32] Convective homogenization of the water column resulting from WDBF is yet another mechanism of steepening of isopycnals under the influence of downwelling-favorable winds, along with the turbulent mixing and cross-shelf advection. *Lentz and Largier* [2006] have shown that advection determines the plume structure for weak downwelling winds, while turbulent mixing becomes dominant as the downwelling wind stress increases. At the coastal current front, convection and wind-driven mixing are expected to be intricately linked, as the convective deepening of the mixed layer creates favorable conditions for shear-driven turbulence and Langmuir cell development [*Li et al.*, 2005]. Relative importance of convection is given by the Hoennikker number [*Li and Garrett*, 1995]:

$$Ho = -\frac{4B}{U_s \beta u_*^2},$$

where B is the surface buoyancy flux, U_s is the Stokes drift velocity at the surface, β is the inverse of the vertical e-folding scale of Langmuir circulation, and $u^* = (\tau/\rho_0)^{1/2}$ is wind stress-related friction velocity in the water. Large-eddy simulation models have shown, that for fully developed seas and neutral stratification, transition from Langmuir and shear-driven turbulence to a convective regime occurs at $Ho \gtrsim 0.8$ [*Li et al.*, 2005]. Parameters of Langmuir circulation can be estimated as $U_s \approx 0.015u$, $\beta \approx (82 \text{ m s}^{-2})u^{-2}$, where u is the wind speed [*Li and Garrett*, 1993]. Considering the wind-driven buoyancy flux obtained above, we estimate that the Hoennikker number at the OCCC front varied between 0.02 and 0.4 during the winter of 2006. Consequently, the structure of mixed layer turbulence in the vicinity of the front can be expected to be substantially modified by convection (at $Ho = 0.4$, the ratio of buoyancy- and wind-driven turbulence intensities is about 1:2 [*Li et al.*, 2005]). The changes of the surface mixed layer structure, in turn alter the cross-shelf Ekman circulation, which may essentially shut down when the water becomes well mixed [*Austin and Lentz*, 2002]. Interconnection between convection, turbulent mixing and advection is further investigated in the next section using numerical modeling.

4. Joint Effects of Wind and Cooling in an Idealized Numerical Model of a Coastal Current

[33] In order to illustrate the evolution of OCCC under the influence of wind forcing and cooling and gain further insight, a simplified two-dimensional numerical model of a coastal current was constructed using the Regional Oceanic Modeling System (ROMS). Details of the model configuration are given in Appendix A. The model set-up mimicked the OCCC structure to facilitate comparison with the observations.

[34] Effects of steady cooling interrupted by periods of moderate downwelling-favorable winds are studied in section 4.1. Wind-driven cross-shelf circulation in the presence and absence of a coastal current front is contrasted in section 4.2.

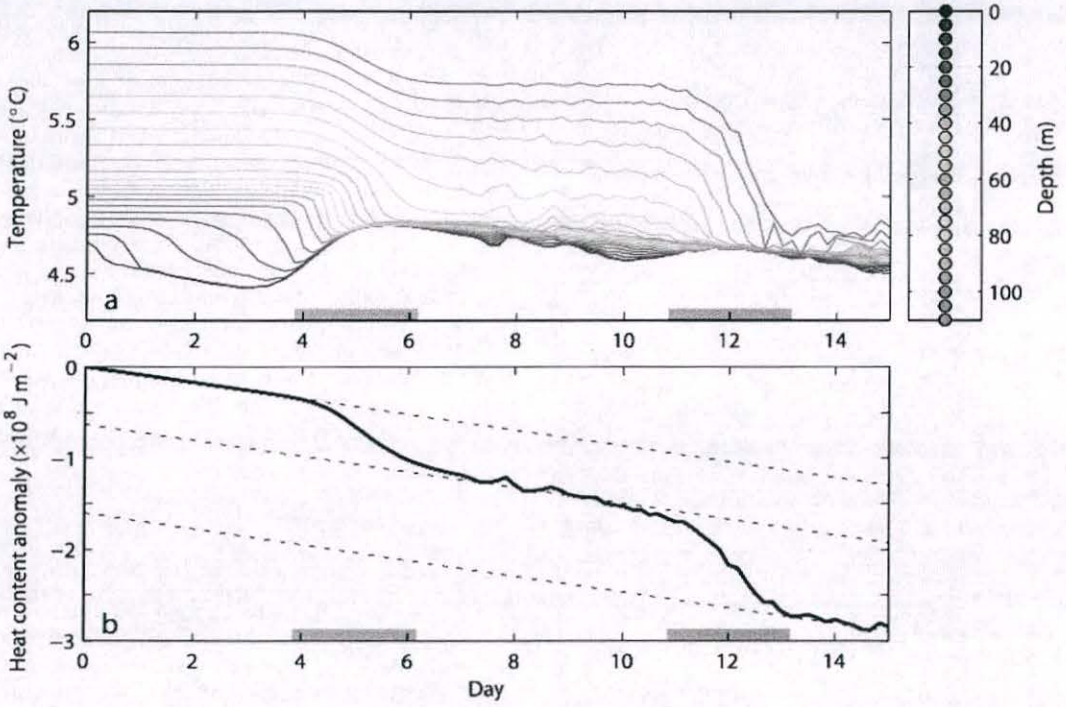

Figure 10. Evolution of (a) temperature and (b) heat content anomaly at a virtual mooring, placed within the model domain 13 km offshore (see Figure 9). (Figure 10a) Temperature at various levels is shown color-coded by depth. Vertical distribution and color-coding of selected levels are also shown. (Figure 10b) Dashed lines correspond to uniform heat loss at a rate of 100 W m^{-2}. Gray shading indicates the downwelling periods with negative wind stress exceeding 0.05 Pa. Compare with Figures 5c and 6.

4.1. Vertical Stratification Response

[35] Destruction of vertical temperature stratification by downwelling winds observed on the Outer Cape Cod (section 3.2, Figures 5a, 5b, and 5c) can be adequately reproduced by the simple two-dimensional model driven by steady cooling and episodic "storms," represented by bursts of downwelling-favorable winds (Figures 9 and 10).

[36] The model clearly shows the contrast between the gradual erosion of the near-surface stratification by cooling during days 0–3 and vigorous destratification driven by WDBF during days 4–6. Mixed layer temperature decreases in the first instance and increases in the second, in accord with both the observations and the heat content considerations (section 3.2). Vertical stratification is further reduced during the downwelling events because of temperature decrease below the mixed layer (60–110 m). This decrease is a result of subduction of cold surface water at the front and its subsequent offshore advection. Pathways of this advection are further discussed in the next section.

[37] During the subsequent downwelling event (days 11–13), vertical stratification is reduced more rapidly and more completely. This can be explained in part by the preconditioning effect of the preceding downwelling event, which deepened the mixed layer and reduced its stratification. As the front location moves offshore with each storm, the virtual mooring was also situated closer to the region of active subduction during the second event. Consequently, the effect of cold water advection was proportionately larger. Similar amplification of the response to consecutive winter storms was observed during the Outer Cape Cod experiment (section 3.2).

[38] A region of low vertical stratification, likely created by the described combination of convection and advection, was commonly observed offshore of the OCCC front (Figure 2d). During the downwelling relaxation phase (situation shown in Figure 2), this weakly stratified region was capped, as the stratification within the coastal current was restored. Convection induced by WDBF during a downwelling event steepens isopycnals and reduces potential vorticity in the coastal current region. Ensuing baroclinic instability is expected to eventually restore the sloping coastal current front once the winds abate. In the two-dimensional formulation used in the model, however, restratification occurs via symmetric instability [*Haine and Marshall*, 1998], which may not occur in the field. Other restratifying factors, namely upstream freshwater input, upwelling-favorable winds, and diurnal heating, were also excluded from the model for simplicity. Consequently, the important issue of the mechanisms of coastal current restratification will not be discussed here, but will be addressed in subsequent studies.

4.2. Cross-Shore Circulation Response

[39] Influence of a coastal current front on the structure of cross-shore circulation can also be illustrated using the simple two-dimensional numerical model. For this purpose,

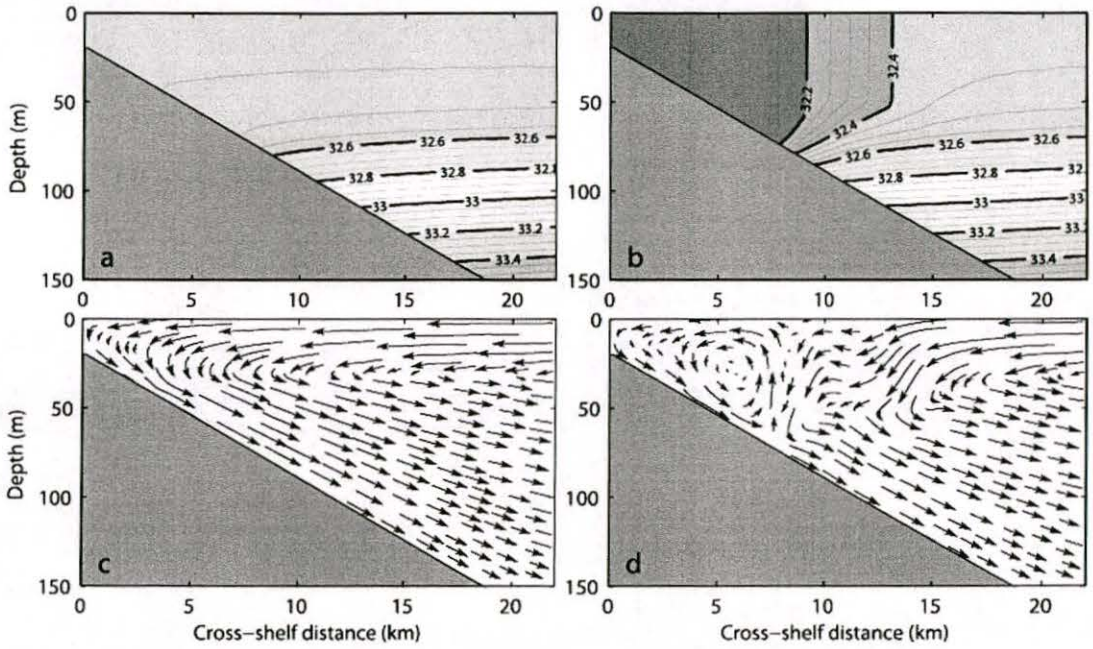

Figure 11. Downwelling response in the (a, c) absence and in the (b, d) presence of the coastal current. Salinity distribution (Figures 11a and 11b) and flow pattern (Figures 11c and 11d) on a cross-shelf section at the peak of the downwelling wind event (day 5) are shown. The length of the arrows represents 24-hour advection in an instantaneous ("frozen") flow field.

two model runs were performed: with and without the freshwater anomaly near the coast, simulating the coastal current (Figures 11a and 11b). Offshore stratification was identical in both cases (see Appendix A for the details). No heat loss was imposed in those runs for simplicity.

[40] Downwelling circulation in the cross-shore plane is primarily driven by onshore Ekman flow near the surface. In deep water, transport of this flow reaches the maximum value of $\tau f_0^{-1} \rho_0^{-1}$, where τ is the wind stress. In the absence of the coastal current (Figures 11a and 11c), frictional transport decays gradually toward the shore, as the water depth becomes comparable with the Ekman layer thickness. Convergence of the wind-driven flow creates a cross-shore pressure gradient that drives downwelling and the return flow along the bottom. This circulation pattern provides effective water exchange between the inner-shelf and mid-shelf zones.

[41] The coastal current density front interrupts the cross-shelf circulation pattern (Figure 11d). Negative wind-driven buoyancy flux at the front increases the thickness of the surface boundary layer, which creates a local convergence of Ekman transport. This effect is similar to the shutdown of the cross-shelf transport on the inner shelf demonstrated by *Austin and Lentz* [2002]. As a result of transport convergence and associated strong downwelling most of the Ekman transport is recirculated offshore of the front. Another much weaker recirculation cell is established inshore of the front. The inner shelf becomes virtually isolated from the offshore advection. On the other hand, the area just offshore of the coastal current front becomes the site of the cold water subduction. Consequently, the outer band of the coastal current (and not the inner shelf) is most likely to be responsible for ventilation of the intermediate water masses of the adjacent basins and setting their properties.

5. Discussion

[42] Wintertime water mass modification on the continental shelf by means of cooling or brine rejection is the leading mechanism for ventilation of intermediate layers of the world's oceans. In the Gulf of Maine, the Maine Intermediate Water (MIW) is believed to be formed in winter in the shallow regions on the western edge of the Gulf [*Brown et al.*, 1977; *Brown and Irish*, 1993; *Hopkins and Garfield*, 1979; *Mupparapu and Brown*, 2002]. The presence of relatively fresh buoyant water carried along the margins of the Gulf by coastal currents, however, reduces the effectiveness of dense water formation in shallow water and its export to the midshelf [*Shcherbina and Gawarkiewicz*, 2008].

[43] Wind-driven buoyancy advection, considered in the present study, may also alter the dynamics and the pathways of the shelf water mass modification. On the one hand, interruption of downwelling circulation by the coastal current, discussed in section 4.2, reduces the effective minimum depth of the basin and consequently the maximum density increase attained by wintertime cooling. On the other hand, subduction offshore of the coastal current front creates a direct connection between the surface and benthic boundary layers. This short-circuit connection (Figure 11d) allows the cold surface water to reach the bottom at 60–100 m depth relatively sooner after the onset

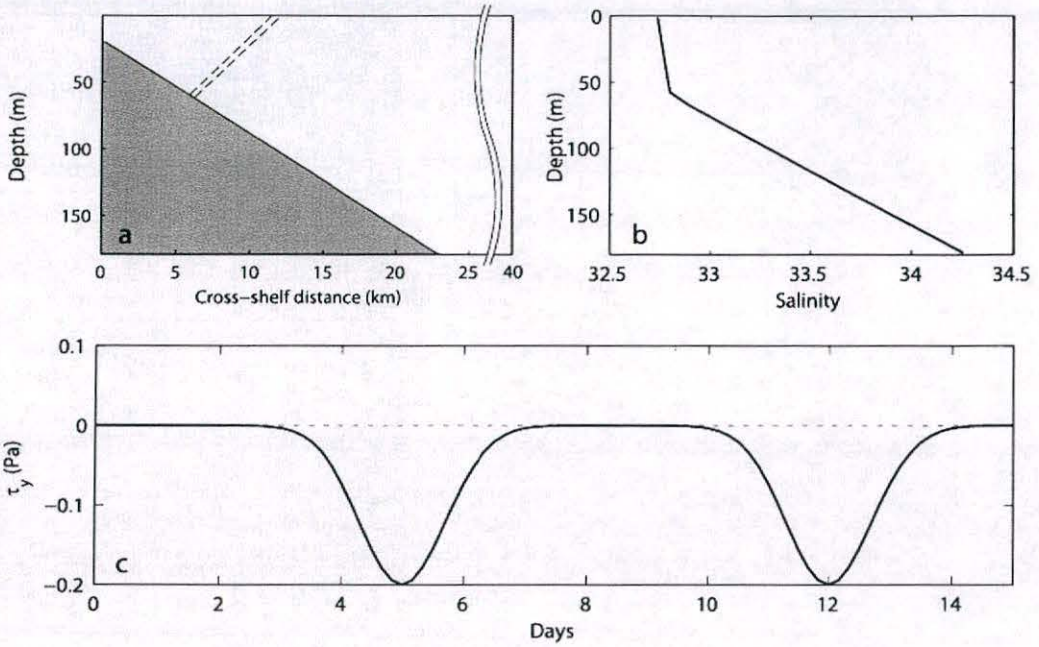

Figure A1. The coastal current model set-up. (a) Cross-section of the model domain. The channel is extended periodically in the direction perpendicular to the image plane. Dashed lines show initial location of coastal current front. (b) Offshore salinity profile. (c) Along-channel wind stress (negative stress corresponds to downwelling-favorable wind).

of the downwelling wind, than in the uniformly stratified case (Figure 11c). The net effect of the described factors on the dense shelf water formation and export is expected to depend on the details of the temperature and salinity stratification, and wind forcing profile. It is also unclear how the combination of wind and buoyancy forcing affects cross-shore eddy fluxes, which are considered to be the primary mechanism of cross-shelf density exchange [*Gawarkiewicz and Chapman*, 1995; *Pringle*, 2001]. Observations suggest that the coastal current plume may exhibit more alongshore variability during the periods of upwelling winds, suggesting reduced stability and enhanced eddy activity [*Fong et al.*, 1997].

[44] Although it is not considered in the present study, the bottom boundary layer (BBL) dynamics are also likely to be affected by the intermittent wind-driven convection and subduction at the CC front. OCCC is a "bottom-trapped" gravity current [*Shcherbina and Gawarkiewicz*, 2008]; as such, it is controlled by the BBL dynamics [*Chapman and Lentz*, 1994]. Overlapping of the surface and bottom boundary layers at the CC front can be expected to further complicate the three-dimensional circulation on the shelf. When such overlap exists, cross-shelf wind stress also becomes an important contributor to the cross-shelf momentum balance [*Tilburg and Garvine*, 2003]. Bottom friction was deliberately excluded from our model in order to simplify the illustration of WDBF effects. Further investigation of its role warrants a separate study.

[45] The interaction of a buoyant current with surface cooling and WDBF, described in this study, can be directly related to the similar processes in the Labrador Sea. *Pickart et al.* [1997] showed that the deep convection within the Labrador Current contributes to the ventilation of a major intermediate water mass of the North Atlantic: the Labrador Seawater (LSW). Additionally, *Straneo et al.* [2002] stressed the importance of WDBF for this overturn. The present study shows that interaction of wind- and buoyancy-driven processes in coastal regions can be substantially stronger than offshore. At the same time, adequate representation of this interaction in large-scale numerical models is further complicated by the shallow water effects (such as changing topography, bottom friction, and terrestrial freshwater input) that need to be carefully considered in future research.

6. Conclusion

[46] Wind-driven buoyancy flux was found to be an important forcing mechanism on the continental shelf east of Cape Cod in winter. Cross-shore gradient of surface density, a necessary condition for development of WDBF, is found at the offshore edge of the Outer Cape Cod Coastal Current which persists throughout the winter. Observed values of the density gradients and wind forcing suggest that WDBF at the coastal current front may substantially exceed surface buoyancy loss associated with seasonal cooling. In December 2005 to March 2006, mean WDBF at the OCCC front exceeded surface buoyancy loss by a factor of 5.

[47] Numerical process modeling suggested that subduction of cold surface water at the coastal current front may interrupt onshore Ekman transport associated with the

downwelling-favorable winds. As a result, the exchange between the inner-shelf and midshelf may be altered.

Appendix A: Model Configuration

[48] The two-dimensional study of cross-shelf circulation was conducted using the Regional Oceanic Modeling System (ROMS). ROMS is a free-surface terrain-following primitive equation ocean circulation model [*Shchepetkin and McWilliams*, 2005].

[49] The model domain is a short periodic meridional channel 40 km wide and 1 km long. The bottom depth increases linearly from 20 m at the western edge of the channel to 180 m 23 km offshore (Figure A1a). The aspect of the sloping bottom section is 7×10^{-3} (7 m over 1 km), which is similar to the average shelf slope off Cape Cod. No-flow, free-slip boundary conditions are imposed at the channel "shores." The Coriolis parameter is $f_0 = 9.8 \times 10^{-5}$ s^{-1}, corresponding to 42°N.

[50] The model employed stratification-dependent realistic mixing. Vertical eddy viscosity and diffusivity were parameterized using the "k-ε" turbulence closure scheme [*Jones and Launder*, 1972]. The scheme was modified to incorporate instantaneous convective adjustment for the case of statically unstable density profile.

[51] The model was initialized with temperature and salinity fields, similar to those observed at the Outer Cape Cod in early winter [*Shcherbina and Gawarkiewicz*, 2008]. Basic stratification consisted of a weakly stratified surface layer in the upper 60 m, overlaying linearly stratified water mass below. Salinity increased from 32.73 at the surface to 32.8 at 60 m, and to 34.25 at 180 m (Figure A1b). Temperature was initially proportional to salinity, on the basis of 15 February 2006 data regression. The resulting buoyancy frequency was $N = 2.6 \times 10^{-3}$ s^{-1} $\approx 26f_0$ in the surface layer and $N = 8.1 \times 10^{-3}$ s^{-1} $\approx 83f_0$ below.

[52] For the runs simulating coastal current structure, initial conditions also included a wedge of relatively fresh and cold water (salinity and temperature anomalies of -0.5 and -1°C, respectively) inshore of the 60-m isobaths. The coastal current front had a characteristic width of 6 km, intersected the surface approximately 12 km offshore, and had a slope of 1.2×10^{-2} (Figure A1a). Vertical stratification within the front reaches $N = 9.8 \times 10^{-3}$ s^{-1} $\approx 100f_0$. The initial velocity field was in geostrophic balance with the frontal stratification.

[53] The model was driven by two bursts of downwelling-favorable wind at days 5 and 12. Wind stress evolution during each burst followed a Gaussian function, with the amplitude of 0.2 N m^{-2} (approximately corresponding to wind speed of 12 m s^{-1}), and characteristic timescale of 2 days (Figure A1c). Duration of wind bursts was chosen after considering decorrelation timescale of the observed wind stress (Figure 5d), which was found to be 22–24 hours (not shown). Uniform heat loss of 100 W m^{-2} was also imposed at the surface.

[54] **Acknowledgments.** We thank Captain Ken Houtler and Chief Mate Ian Hanley for getting *Tioga*, REMUS, and ourselves through some rough seas; Craig Marquette for designing and deploying the moorings; Leif Thomas for much stimulating discussion; Chris Linder, Frank Bahr, and Al Plueddemann for assisting in field studies; and two anonymous reviewers for their comments. This work was supported by the Coastal Ocean Institute of the Woods Hole Oceanographic Institution and the WHOI SeaGrant Office under grant NA06OAR4170021. G.G. was supported by the Office of Naval Research as part of the AWACS program under grant N00014-05-1-0410. A.S. was supported, in part, by WHOI Post-Doctoral Scholarship.

References

Austin, J. A., and S. J. Lentz (2002), The inner shelf response to wind-driven upwelling and downwelling, *J. Phys. Oceanogr.*, *32*(7), 2171–2193, doi:10.1175/1520-0485(2002)032<2171:TISRTW>2.0.CO;2.

Brown, W. S., and J. D. Irish (1993), The annual variation of water mass structure in the Gulf of Maine: 1986–1987, *J. Mar. Res.*, *51*(1), 53–107, doi:10.1357/0022240933223828.

Brown, W. S., J. Vermersch, and R. C. Beardsley (1977), Wintertime 1974–75 Western Gulf of Maine Experiment data, *Tech. Rep. WHOI-77-22*, Woods Hole Oceanogr. Inst., Woods Hole, Mass.

Chapman, D. C., and S. J. Lentz (1994), Trapping of a coastal density front by the bottom boundary layer, *J. Phys. Oceanogr.*, *24*(7), 1464–1479, doi:10.1175/1520-0485(1994)024<1464:TOACDF>2.0.CO;2.

Fairall, C. W., E. F. Bradley, J. E. Hare, A. A. Grachev, and J. B. Edson (2003), Bulk parameterization of air-sea fluxes: Updates and verification for the COARE algorithm, *J. Clim.*, *16*(4), 571–591, doi:10.1175/1520-0442(2003)016<0571:BPOASF>2.0.CO;2.

Fong, D. A., and W. R. Geyer (2001), Response of a river plume during an upwelling favorable wind event, *J. Geophys. Res.*, *106*(C1), 1067–1084, doi:10.1029/2000JC900134.

Fong, D. A., W. R. Geyer, and R. P. Signell (1997), The wind-forced response on a buoyant coastal current: Observations of the western Gulf of Maine plume, *J. Mar. Syst.*, *12*(1–4), 69–81.

Franks, P., and D. Anderson (1992), Alongshore transport of a toxic phytoplankton bloom in a buoyancy current: *Alexandrium tamarense* in the Gulf of Maine, *Mar. Biol. Berlin*, *112*, 165–174, doi:10.1007/BF00349740.

Garvine, R. W. (1996), Buoyant coastal discharge on the inner continental shelf: A frontal model, *J. Mar. Res.*, *54*(1), 1–33, doi:10.1357/0022240963213457.

Gawarkiewicz, G., and D. Chapman (1995), A numerical study of dense water formation and transport on a shallow, sloping continental shelf, *J. Geophys. Res.*, *100*(C3), 4489–4507, doi:10.1029/94JC01742.

Geyer, W. R., R. P. Signell, D. A. Fong, J. Wang, D. M. Anderson, and B. A. Keafer (2004), The freshwater transport and dynamics of the western Maine coastal current, *Cont. Shelf Res.*, *24*(12), 1339–1357, doi:10.1016/j.csr.2004.04.001.

Haine, T. W. N., and J. C. Marshall (1998), Gravitational, symmetric and baroclinic instability of the ocean mixed layer, *J. Phys. Oceanogr.*, *28*(4), 634–658, doi:10.1175/1520-0485(1998)028<0634:GSABIO>2.0.CO;2.

Hetland, R. D. (2005), Relating river plume structure to vertical mixing, *J. Phys. Oceanogr.*, *35*(9), 1667–1688, doi:10.1175/JPO2774.1.

Hill, A. E. (1998), Buoyancy effects in coastal and shelf seas, in *The Sea*, vol. 10, edited by K. H. Brink and A. R. Robinson, pp. 21–62, John Wiley, Hoboken, N. J.

Hopkins, T. S., and N. Garfield (1979), Gulf of Maine intermediate water, *J. Mar. Res.*, *37*(1), 103–109.

Houghton, R. W., C. E. Tilburg, R. W. Garvine, and A. Fong (2004), Delaware River plume response to a strong upwelling-favorable wind event, *Geophys. Res. Lett.*, *31*, L07302, doi:10.1029/2003GL018988.

Jones, W. P., and B. E. Launder (1972), The prediction of laminarization with a two-equation model of turbulence, *Int. J. Heat Mass Transfer*, *15*, 301–314, doi:10.1016/0017-9310(72)90076-2.

Lentz, S. (2004), The response of buoyant coastal plumes to upwelling-favorable winds, *J. Phys. Oceanogr.*, *34*(11), 2458–2469, doi:10.1175/JPO2647.1.

Lentz, S., and K. Helfrich (2002), Buoyant gravity currents along a sloping bottom in a rotating fluid, *J. Fluid Mech.*, *464*, 251–278, doi:10.1017/S0022112002008868.

Lentz, S. J., and J. Largier (2006), The influence of wind forcing on the Chesapeake Bay buoyant coastal current, *J. Phys. Oceanogr.*, *36*(7), 1305–1316, doi:10.1175/JPO2909.1.

Li, M., and C. Garrett (1993), Cell merging and jet/downwelling ratio in Langmuir circulation, *J. Mar. Res.*, *51*(4), 737–769, doi:10.1357/0022240933223945.

Li, M., and C. Garrett (1995), Is Langmuir circulation driven by surface waves or surface cooling?, *J. Phys. Oceanogr.*, *25*(1), 64–76, doi:10.1175/1520-0485(1995)025<0064:ILCDBS>2.0.CO;2.

Li, M., C. Garrett, and E. Skyllingstad (2005), A regime diagram for classifying turbulent large eddies in the upper ocean, *Deep Sea Res., Part I*, *52*, 259–278, doi:10.1016/j.dsr.2004.09.004.

Mupparapu, P., and W. S. Brown (2002), Role of convection in winter mixed layer formation in the Gulf of Maine, February 1987, *J. Geophys. Res.*, *107*(C12), 3229, doi:10.1029/1999JC000116.

Pickart, R. S., M. A. Spall, and J. R. N. Lazier (1997), Mid-depth ventilation in the western boundary current system of the sub-polar gyre, *Deep Sea Res., Part I, 44*, 1025–1054, doi:10.1016/S0967-0637(96)00122-7.

Pringle, J. M. (2001), Cross-shelf eddy heat transport in a wind-free coastal ocean undergoing winter time cooling, *J. Geophys. Res., 106*(C2), 2589–2604, doi:10.1029/2000JC900148.

Shchepetkin, A. F., and J. C. McWilliams (2005), The regional oceanic modeling system: A split-explicit, free-surface, topography-following-coordinate ocean model, *Ocean Modell., 9*, 347–404, doi:10.1016/j.ocemod.2004.08.002.

Shcherbina, A. Y., and G. G. Gawarkiewicz (2008), A coastal current in winter: Autonomous underwater vehicle observations of the coastal current east of Cape Cod, *J. Geophys. Res., 113*, C07030, doi:10.1029/2007JC004306.

Smith, P. C., and J. I. MacPherson (1987), Cross-shore variations of near-surface wind velocity and atmospheric turbulence at the land-sea boundary during CASP, *Atmos. Ocean, 25*(3), 279–303.

Straneo, F., M. Kawase, and R. S. Pickart (2002), Effects of wind on convection in strongly and weakly baroclinic flows with application to the Labrador Sea, *J. Phys. Oceanogr., 32*(9), 2603–2618.

Thomas, L. N. (2005), Destruction of potential vorticity by winds, *J. Phys. Oceanogr., 35*(12), 2457–2466, doi:10.1175/JPO2830.1.

Tilburg, C. E., and R. W. Garvine (2003), Three-Dimensional flow in a shallow coastal upwelling zone: Alongshore convergence and divergence on the New Jersey Shelf, *J. Phys. Oceanogr., 33*(10), 2113–2125, doi:10.1175/1520-0485(2003)033<2113:TFIASC>2.0.CO;2.

Whitney, M. M., and R. W. Garvine (2005), Wind influence on a coastal buoyant outflow, *J. Geophys. Res., 110*, C03014, doi:10.1029/2003JC002261.

Yu, L. S., R. A. Weller, and B. M. Sun (2004), Improving latent and sensible heat flux estimates for the Atlantic Ocean (1988–99) by a synthesis approach, *J. Clim., 17*(2), 373–393, doi:10.1175/1520-0442(2004)017<0373:ILASHF>2.0.CO;2.

G. G. Gawarkiewicz, Woods Hole Oceanographic Institution, 266 Woods Hole Road, Woods Hole, MA 02543, USA.

A. Y. Shcherbina, Applied Physics Laboratory, University of Washington, Seattle, WA 98105, USA. (ashcherbina@apl.washington.edu)